

# On the Suppression and Enhancement of Thermal Chemical Rates in a Cavity

Jing Sun\* and Oriol Vendrell\*

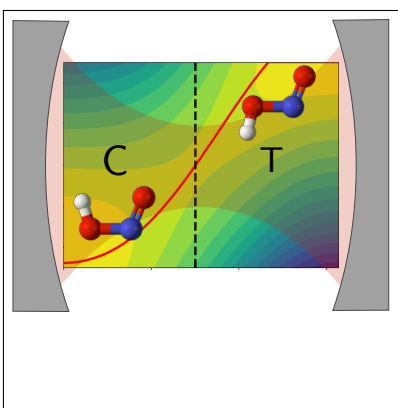
*Theoretische Chemie, Physikalisch-Chemisches Institut, Universität Heidelberg,  
69120 Heidelberg, Germany*

E-mail: [jing.sun@pci.uni-heidelberg.de](mailto:jing.sun@pci.uni-heidelberg.de); [oriol.vendrell@uni-heidelberg.de](mailto:oriol.vendrell@uni-heidelberg.de)

## Abstract

The observed modification of thermal chemical rates in Fabry-Perot cavities remains a poorly understood effect theoretically. Recent breakthroughs explain some of the observations through the Grote-Hynes theory, where the cavity introduces friction with the reaction coordinate, thus reducing the transmission coefficient and the rate. The regime of rate enhancement, the observed sharp resonances at varying cavity frequencies, and the survival of these effects in the collective regime remain mostly unexplained. In this paper, we consider the *cis-trans* isomerization of HONO atomistically using an *ab-initio* potential energy surface. We evaluate the transmission coefficient using the reactive flux method and identify the conditions for rate acceleration. In the under-damped, low-friction regime of the reaction coordinate, the cavity coupling enhances the rate with increasing coupling strength until reaching the Kramers turnover point. Sharp resonances in this regime are related to cavity-enabled energy redistribution channels.

## Graphical TOC Entry



Vibrational strong coupling (VSC) has emerged as a very active front in the field of polaritonic chemistry since the pioneering demonstrations of Rabi splitting in the infrared domain in Fabry-Perot configurations.<sup>1-3</sup> At the core of this sub-discipline lies the promise of modifying,<sup>4</sup> and ultimately controlling<sup>5</sup> the mechanisms and rates of thermal chemical reactions using the vacuum fields of cavities.<sup>6</sup> Besides important breakthroughs in the linear and non-linear spectroscopy of VSC systems,<sup>4-7</sup> the more spectacular results remain the experiments reporting the modification of chemical rates in cavities by the Ebbesen group and others.<sup>8-13</sup> These experiments have triggered the proposal of several theoretical models to explain how the cavity modifies the ground electronic state structure<sup>14</sup> and spectroscopy<sup>15</sup> and, more recently, how it modifies reaction rates.<sup>16-21</sup>

Theoretical models based on the Grote-Hynes theory<sup>22</sup> predict the suppression of the transmission coefficient with increasing cavity coupling due to increased friction at the top of the reaction barrier.<sup>19-21</sup> How cavities can enhance chemical reactions,<sup>9</sup> how sharp resonances of the cavity with vibrational modes affect the mechanism,<sup>9,10</sup> and how these effects survive in the collective VSC regime, have remained poorly understood questions.

Here, we simulate the rate of a realistic isomerization reaction atomistically using an *ab initio* potential, both for one and several HONO molecules, in the VSC regime. Our simulations explain how the cavity enhances chemical rates in the underdamped regime and capture the turnover from the underdamped to the damped regime as a function of the cavity coupling strength. Moreover, we explain how, in the underdamped regime, sharp resonances of the cavity with vibrational modes can strongly affect the reaction rate. Finally, our results show how, in the collective VSC regime, the strong direct coupling to the reaction coordinate ceases to be the determining factor in the cavity effect.

Our starting point is the Hamiltonian for a molecular ensemble coupled to one or several cavity modes

$$\hat{H} = \sum_{l=1}^N \hat{H}_{mol}^{(l)} + \hat{H}_{cav} \quad (1)$$

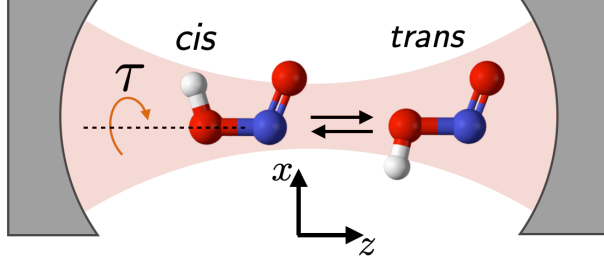


Figure 1: *cis-trans* isomerization reaction in HONO. The axes indicate the body-fixed frame of the molecules in the simulation. The presence of the cavity is indicated schematically and is not to scale. HONO is characterized by 6 vibrational coordinates: 3 stretching modes, O–H, O–N and N=O; 2 bending modes, H–O–N and O–N=O; 1 torsion mode  $\tau$ , the isomerization reaction coordinate.

with

$$\hat{H}_{mol}^{(l)} = \sum_{j_l=1}^F \frac{\hat{P}_{j_l}^2}{2M_{j_l}} + \hat{V}(R_{1_l} \dots R_{F_l}), \quad (2)$$

$$\hat{H}_{cav} = \frac{1}{2} \left[ \hat{p}_{cav}^2 + \omega_{cav}^2 \left( \hat{q}_{cav} + \frac{\lambda}{\omega_{cav}} \cdot \sum_{l=1}^N \hat{\boldsymbol{\mu}}^{(l)} \right)^2 \right], \quad (3)$$

and where  $V(R_{1_l} \dots R_{F_l})$  denotes the ground electronic state potential energy surface (PES) of the  $l$ -th molecule with momenta  $P_{j_l}$  and positions  $R_{j_l}$ . Hence, the Born-Oppenheimer (BO) approximation is assumed within each molecule, and  $\boldsymbol{\mu}^{(l)} \equiv \boldsymbol{\mu}^{(l)}(R_{1_l} \dots R_{F_l})$  is the permanent dipole vector of the  $l$ -th molecule.  $\hat{H}_{cav}$  can be reached from the Coulomb-gauge light-matter interaction Hamiltonian by taking the long wave approximation followed by a unitary transformation to the length form.<sup>17,23,24</sup> For later convenience, we write  $\hat{H}_{cav}$  in its position-momentum representation  $(\hat{q}_{cav}, \hat{p}_{cav})$ .  $\omega_{cav}$  corresponds to the cavity mode frequency. This form of the light-matter interaction has become standard in most theoretical studies of VSC,<sup>17,19,20,25</sup> and details on its derivation<sup>23,26</sup> and properties<sup>27</sup> can be found elsewhere. The parameter  $\lambda$  equals the coupling strength  $\lambda = \sqrt{1/\epsilon_0 V}$  times the unit polarization vector  $\boldsymbol{\epsilon}$  of the cavity mode, and  $V$  represents the cavity volume.<sup>23</sup> Similarly to other studies and to facilitate comparisons, we introduce the coupling parameter  $g = \lambda\sqrt{\hbar\omega_{cav}/2}$ , which has units of electric field (using this relation and  $\hat{q}_{cav} = \sqrt{\hbar/2\omega_{cav}}(\hat{a}^\dagger + \hat{a})$ , the linear coupling

term in  $\hat{H}_{cav}$  reads  $g \boldsymbol{\epsilon} \cdot \boldsymbol{\mu} (\hat{a}^\dagger + \hat{a})$ .

The simplicity of the unimolecular reaction mechanism in HONO makes it an ideal benchmark system to understand how dynamical cavity effects can modify chemical rates as compared, e.g., to bimolecular reactions in solution.<sup>10,28</sup> We base our study on the CCSD(T)-quality *ab initio* potential energy surface (PES) of Richter et al.,<sup>29</sup> which features a reaction barrier height of about 0.51 eV (49 kJ/mol) and where the *trans* isomer is 11 meV more stable than the *cis* one. Quantum dynamics studies of the HONO isomerization triggered by strong laser pulses have been based on this PES.<sup>30,31</sup> Despite its simplicity, this chemical reaction constitutes a fully coupled and rich dynamical system. Similarly to other isomerization reactions, e.g. involving hydrocarbons,<sup>32-34</sup> it takes place in the underdamped regime. Throughout this work, the molecules are kept at a fixed orientation with respect to the polarization direction of the cavity mode. In this way, we focus on the coupling of the  $\mu_x$  dipole component to the cavity polarizaton. As shown in the SI, this component of the molecular dipole has the strongest modulation at the isomerization barrier configuration.

The molecule-cavity system is considered within the classical approximation, thus transforming all coordinate operators in Hamiltonians 2 and 3 to classical functions. A classical description of the VSC regime is not new and has been successfully applied to bulk systems described by force-field potentials<sup>35</sup> and model Hamiltonians.<sup>19,36</sup> The *cis-trans* reaction rate is described with the reactive flux method for the classical rate constant<sup>32-34,37,38</sup>

$$K(t) = x_{cis}^{-1} \langle \dot{\tau}(0) \delta[\tau(0) - \tau^\ddagger] \theta[\tau(t)] \rangle, \quad (4)$$

where  $x_{cis}$  is the equilibrium fraction of HONO at the *cis* geometry,  $\dot{\tau}(0)$  is the initial velocity of a phase-space point perpendicular to the dividing surface between reactants and products, and  $\tau^\ddagger$  is the torsion angle corresponding to the transition state (TS) geometry. The brackets indicate the canonical ensemble average over trajectories, where we considered a temperature of 300 K throughout. The Heaviside function  $\theta[\tau]$  is defined to be one for

the *trans* configurations, and zero otherwise. The exact reactive flux is obtained in the limit  $t \rightarrow \infty$ , in practice when the plateau for  $K(t)$  is reached.<sup>38</sup> This occurs when all classical trajectories starting from the dividing surface become trapped at either the reactants or products side. For example, for the isomerization reaction of *n*-butane in the low-friction environment of a van der Waals liquid this relaxation time is about 1 ps.<sup>33</sup> Now, since<sup>37</sup>

$$\lim_{t \rightarrow 0^+} K(t) = K_{TST}, \quad (5)$$

one can introduce a transmission coefficient  $\kappa(t) = K(t)/K_{TST}$  as the quotient of the numerically exact reactive flux and the reactive flux without recrossing, i.e. the TST assumption.  $K_{TST}$  can be evaluated conveniently using Eyring’s equation,<sup>39,40</sup> while  $\kappa(t)$  is obtained from classical trajectories. As shown in the SI, and as has been discussed in other works,<sup>17,18</sup>  $K_{TST}$  is, to a very good approximation, insensitive to cavity effects. Therefore, we consider  $K_{TST}$  to be completely cavity-independent and describe the cavity effect on the rate as

$$K_{cav} = \kappa_{cav} \kappa_0 K_{TST}, \quad (6)$$

where  $K_0 \equiv \kappa_0 K_{TST}$  is the formally exact classical rate outside the cavity. Here and in the following, transmission coefficients and rate constants without a time argument refer to their plateau value. Clearly, both  $\kappa$  and  $\kappa_0$  lie in the  $[0, 1]$  range but  $\kappa_{cav}$  can be both larger or smaller than one, corresponding to a chemical rate enhancement or suppression, respectively.

In the following, we theoretically demonstrate that both enhancement and suppression of reaction rates are possible within a cavity for realistic chemical processes. Although we rely on classical rate theory,<sup>40</sup> we note that tunneling corrections for hydrogen abstraction reactions at 300 K result in variations of the rate within the same order of magnitude.<sup>41</sup> For reactions involving heavier elements, quantum corrections to the rates are even more insignificant. Along these lines, there is no reason to assume, a priori, that photonic modes with frequencies similar to the atomic vibrations, and in thermal equilibrium, shall result

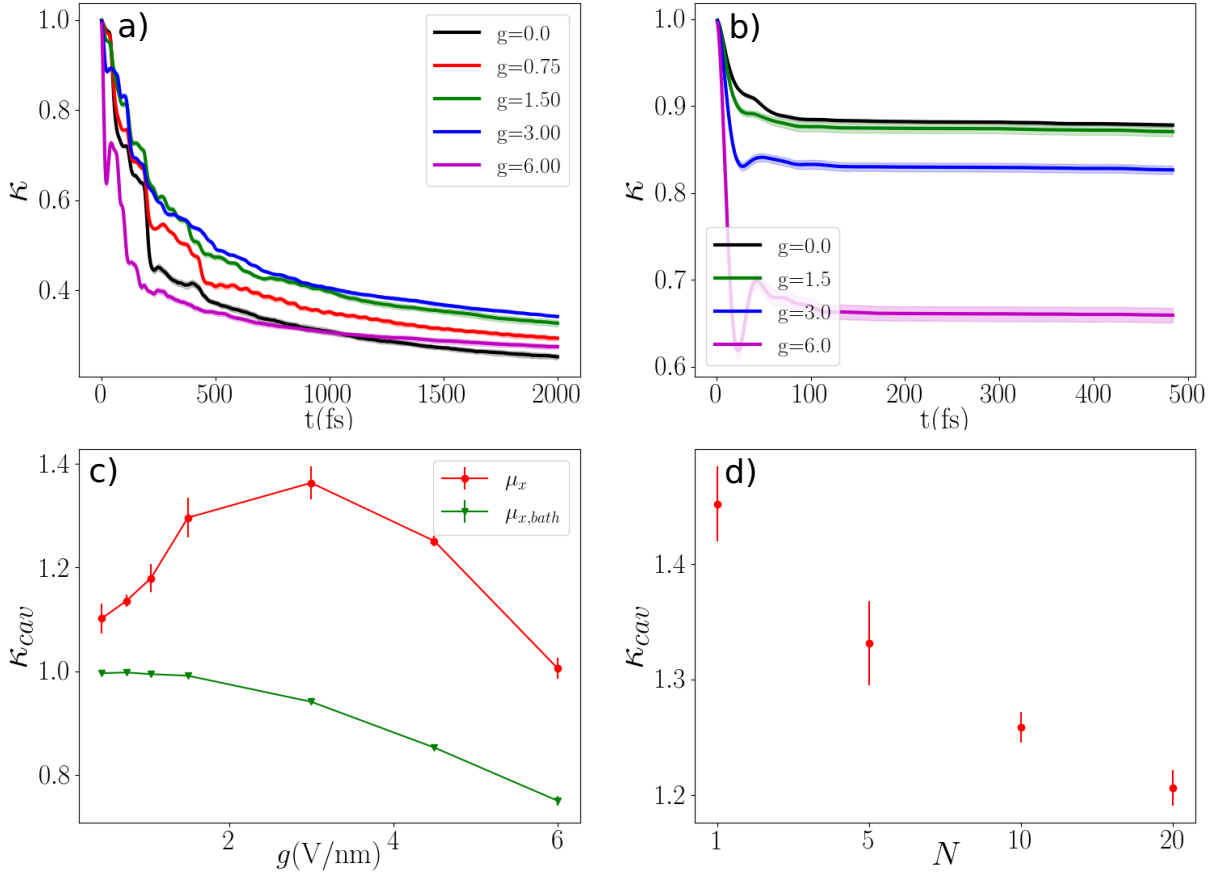


Figure 2: a) Transmission coefficient  $\kappa(t)$  for various cavity-coupling strengths  $g$  (V/nm) for  $N = 1$  and the cavity polarization aligned with HONO's  $x$ -axis. b) same as a) but with the HONO molecules coupled to a bath (see SI). The shaded area on top of the solid lines indicates the standard deviation of the average over trajectory runs. c) Asymptotic  $\kappa_{cav} = \kappa/\kappa_0$  for the curves in a) (red) and b) (green). d)  $\kappa_{cav}$  for increasing number of molecules at constant total polaritonic coupling (see text for details).

in significant quantum effects that affect the general conclusions derived from classical rate theories for VSC systems. This does not exclude situations where quantum effects may be important for quantitative descriptions of cavity-modified rates in reactions involving light atoms, as it is sometimes the case for rates outside cavities.<sup>41–43</sup>

Let us consider a single HONO molecule coupled to a cavity mode with  $x$  polarization with respect to the molecular frame. In this case, the variation of the permanent dipole is largest at the transition state (TS) of the reaction coordinate,  $\tau^\ddagger \approx \pi/2$ . Outside the cavity,  $\kappa_0 \approx 0.35$  at 300 K, the plateau value of the black curve in Fig. 2a. This relatively low transmission

is caused by a slow rate of intra-molecular vibrational energy redistribution (IVR) of the activated trajectories in the underdamped regime. As the cavity-coupling increases, one sees how the plateau value stabilizes at a larger total transmission  $\kappa$  in the red, blue and green curves. The cavity accelerates the chemical reaction by increasing the total transmission coefficient compared to  $\kappa_0$ , i.e.  $\kappa_{cav} > 1$ . This is illustrated by the red trace in Fig. 2c in the coupling regime where  $\kappa_{cav}$  increases, and it is well understood within our theoretical framework: the cavity provides an extra energy redistribution pathway for a system with a low-friction reaction coordinate. Recrossing events are increasingly suppressed and the transmission increases. Nonetheless, as the cavity coupling to the torsion coordinate further increases, a turning point is reached for  $g > 3$  V/nm. The amount of recrossing at the barrier keeps increasing as well, thus finally reverting the trend and decreasing the transmission again. This is the well-known Kramers turning point,<sup>22</sup> which, e.g., was predicted long ago for the isomerization of cyclohexane as a function of solvent viscosity.<sup>34</sup> Figure 2a illustrates its origin in the quick drop of  $\kappa(t)$  at short times for the strongest cavity coupling.

When adding an external bath to HONO (see SI for details), the regime of validity of the GH theory is restored. Figure 2b shows how now  $\kappa(t)$  quickly reaches the plateau value within a few tens of femtoseconds, meaning that activated trajectories visit the region of the TS only once or twice. Since the plateau is reached quickly, the cavity can only have a short-time effect close to the top of the barrier, where it can increase the amount of recrossing thus reduce the transmission coefficient. As illustrated in Fig.2c by the green trace, now  $\kappa_{cav} < 1$  and the chemical rate is reduced for all coupling strengths. This is the regime captured in Refs. 19–21.

A question mark remains still in connection with the collective VSC regime, where most experiments reporting modifications of chemical rates in Fabry-Perot configurations operate. To shed some light into this issue, we have performed trajectory calculations of the transmission coefficient for an increasing number of molecules  $N$  coupled to the cavity, again without an extra bath. The coupling per molecule is scaled as usual by a factor  $N^{-1/2}$  as a means



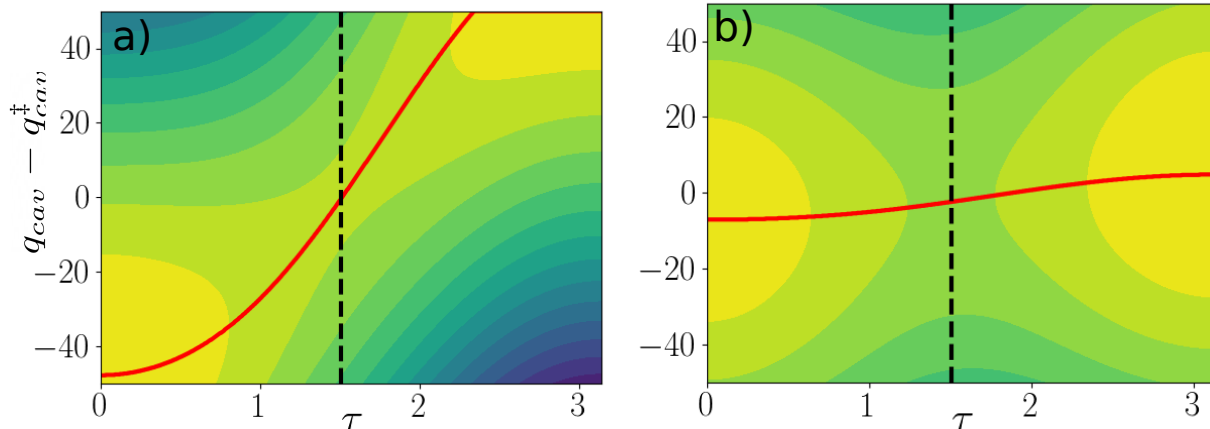


Figure 3: Potential energy surface cut for a) 1 and b) 100 HONO molecules as a function of the reaction coordinate  $\tau$  and the cavity displacement  $q_{cav} - q_{cav}^\ddagger$ . For  $N = 1$  the light-matter coupling is  $g = 8$  V/nm. The cavity coupling in b) is scaled by  $1/\sqrt{N}$  to keep a constant overall light-matter interaction. The color levels start at 0 for the lightest tone and increase in steps of 0.2 eV. The red line indicates the minimum energy path. The vertical dashed line separates the *cis* and *trans* configurations.

to keep the overall light-matter coupling constant.<sup>44</sup> Starting from  $N = 1$ ,  $g = 1$  V/nm, and  $\omega_{cav} = 852$  cm<sup>-1</sup>, one sees in Fig. 2d how, for increasing  $N$ , the cavity effect gradually fades away. Responsible for the gradual trend  $\kappa_{cav} \rightarrow 1$  is the decoupling of the reaction coordinate from the cavity displacement with increasing  $N$ , as seen by comparing the curvature of the minimum energy path (MEP) in Figs. 3a,  $N = 1$ , and 3b, with  $N = 100$ . This reduction of the MEP curvature as  $N$  increases, and thus the reduced friction caused by the cavity, implies that in the large  $N$  limit the cavity is not able to “cage” the TS and induce a decrease of the transmission coefficient through this mechanism.

Finally, we address the question of sharp resonant effects, meaning when the modification of chemical rates is particularly pronounced at specific cavity frequencies. Through trajectory calculations it has been observed that the outcome of reactive events can depend on the resonance between the cavity and vibrational modes of the molecule, but a link to the actual modification of chemical rates has not been established.<sup>25,45</sup> Our simulations of the transmission coefficient in the underdamped, slow IVR regime reveal sharp resonances in the rate constant effect as a function of  $\omega_{cav}$ . As already discussed, in this regime the effect

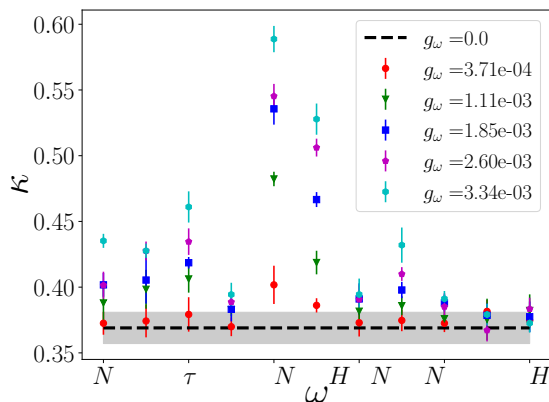


Figure 4: Transmission coefficient  $\kappa$  for various coupling strengths  $g_\omega = g\mu_x^\ddagger/\omega_{cav}$  as a function of  $\omega_{cav}$ . Vertical bars represent standard deviations over the run trajectories.  $\omega_{cav}$  is chosen to be resonant with fundamental modes of molecule:  $\omega_{ONO} = 609(cm^{-1})$ ,  $\omega_\tau = 640(cm^{-1})$ ,  $\omega_{ON} = 852(cm^{-1})$ ,  $\omega_{HON} = 1263(cm^{-1})$ ,  $\omega_{NO} = 1641(cm^{-1})$ ,  $\omega_{OH} = 3426(cm^{-1})$  and with the average of every consecutive pair. The black dashed line indicates  $\kappa_0$  outside the cavity with its standard deviation.

of the cavity is to introduce extra energy redistribution pathways, whereby the effect at short times while passing the TS barrier region is not so important. Thus, when the cavity is resonant with a vibrational mode that happens to be strongly coupled to the reaction coordinate, the enhancement of the rate is more prominent. As seen in Fig. 4,  $\kappa_{cav} \approx 2$  when  $\omega_{cav}$  is resonant with the O-N stretching mode at  $852\text{ cm}^{-1}$ . This is not surprising. It is well-known that the O-N stretch is strongly coupled to the torsion coordinate in HONO:<sup>29,30</sup> Selective laser excitations of this mode result in an enhanced probability of isomerization out of equilibrium.<sup>31</sup> This brings us to the observed cavity catalysis of a unimolecular dissociation in solution by the Ebbesen group.<sup>9</sup> A plausible explanation is that the strong resonance of the cavity mode with a carbonyl group could stabilize the hot nascent products inside the solvent pocket, in this way preventing recrossing events at early times after passage over the TS. Further studies will be required to test our hypothesis.

Let us recapitulate and place our findings in the context of the current literature on thermal rate models in cavities. The regime considered in model studies is the one in which the cavity is strongly coupled to the reaction coordinate, while reactants and products

are strongly damped by a bath<sup>19</sup> or effectively by a short propagation time that hinders recrossing.<sup>14</sup> In this case, the reaction pathway becomes curved, as seen in the Shin-Metieu and other 1D models.<sup>14,19,21</sup> The regime in which the coupling is strong at the barrier top and the reactants and products are damped by a bath is well captured by the Grote-Hynes (GH) theory<sup>22</sup> and has been the basis of theoretical proposals for the reduction of chemical rates in cavities.<sup>19-21</sup> In this regime there are no sharp resonance effects, although there is a continuous dependence of  $\kappa$  on  $\omega_{cav}$  related to the frequency of the inverted reaction barrier.<sup>21</sup> Similarly to our findings, existing theories report a reduction of the transmission coefficient in the collective regime as  $N$  increases (cf. Fig. 2a in Ref. 21). Reference 20 attributes the persistence of the modification of chemical rates in the large  $N$  collective regime to the assumption that “the polariton state is thermally activated to yield collective barrier crossing”.<sup>20</sup> While a coherent superposition of activated complexes may display this behavior, a physical mechanism by which a polaritonic system spontaneously results in coherence in the dark and under thermal equilibrium of the material and photonic modes, has not been put forward.

Concluding, our main contribution has been to identify dynamical effects played by the cavity in the low-friction (or underdamped) regime of the reaction coordinate. In this regime, the cavity effect is twofold: (1) It *accelerates* the chemical rate by increasing the friction compared to the cavity-free system. This reduces the recrossing due to trajectories that, otherwise, would visit reactants and products several times, thus increasing the transmission coefficient compared to  $\kappa_0$ . As the cavity coupling keeps increasing, the overall increased friction can introduce again more coupling at the barrier and the trend can overturn. This is the well-known Kramers turnover situation, and this regime can exist in the condensed phase.<sup>22,34</sup> (2) In the low-friction regime, sharp resonant effects are possible. These are related to the new IVR pathways offered by the cavity. In the products-side, they dissipate energy from the nascent hot products. In the reactants-side, the resonances funnel energy into the nascent activated complexes. Numerically, the former is captured by trajectories

starting towards the products-side and being effectively captured there. The latter is captured by the trajectories initially moving towards reactants and being effectively captured as well. If this reactants-side capture would be ineffective, they would be counted as products but with a negative contribution to the flux, in this way lowering the transmission (cf. Eq. 4). Finally, when a bath is added to the HONO molecule and the overall friction is sufficiently increased, the model reverts to the already known GH regime where the cavity only affects the recrossings at the top of the reaction barrier. Our findings shed important new light onto the question of cavity-modified reactivity. However, it still remains for future work to better understand how these cavity effects can survive in actual liquid phases and in the collective regime for truly macroscopic numbers of molecules. It is plausible that the more detailed answers lie beyond models of independent molecules and may require studies of the transmission coefficient with full consideration of environmental effects in the bulk.<sup>46</sup>

## References

- (1) Hutchison, J. A.; Schwartz, T.; Genet, C.; Devaux, E.; Ebbesen, T. W. *Angew. Chem.* **2012**, *124*, 1624–1628.
- (2) Shalabney, A.; George, J.; Hutchison, J.; Pupillo, G.; Genet, C.; Ebbesen, T. W. *Nat Commun* **2015**, *6*, 5981.
- (3) Ebbesen, T. W. *Acc. Chem. Res.* **2016**, *49*, 2403–2412.
- (4) Dunkelberger, A. D.; Spann, B. T.; Fears, K. P.; Simpkins, B. S.; Owrutsky, J. C. *Nat. Commun.* **2016**, *7*, 13504.
- (5) Yang, Z.; Xiang, B.; Xiong, W. *ACS Photonics* **2020**, *7*, 919–924.
- (6) Dunkelberger, A. D.; Davidson, R. B.; Ahn, W.; Simpkins, B. S.; Owrutsky, J. C. *J. Phys. Chem. A* **2018**, *122*, 965–971.

- (7) Fassioli, F.; Park, K. H.; Bard, S. E.; Scholes, G. D. *J. Phys. Chem. Lett.* **2021**, *12*, 11444–11459.
- (8) Thomas, A. et al. *Angew. Chem. Int. Ed.* **2016**, *55*, 11462–11466.
- (9) Lather, J.; Bhatt, P.; Thomas, A.; Ebbesen, T. W.; George, J. *Angew. Chem. Int. Ed.* **2019**, *58*, 10635–10638.
- (10) Thomas, A. et al. *Science* **2019**, *363*, 615–619.
- (11) Vergauwe, R. M. A.; Thomas, A.; Nagarajan, K.; Shalabney, A.; George, J.; Chervy, T.; Seidel, M.; Devaux, E.; Torbeev, V.; Ebbesen, T. W. *Angew. Chem. Int. Ed.* **2019**, *58*, 15324–15328.
- (12) Thomas, A.; Jayachandran, A.; Lethuillier-Karl, L.; Vergauwe, R. M. A.; Nagarajan, K.; Devaux, E.; Genet, C.; Moran, J.; Ebbesen, T. W. *Nanophotonics* **2020**, *9*, 249–255.
- (13) Imperatore, M. V.; Asbury, J. B.; Giebink, N. C. *J. Chem. Phys.* **2021**, *154*, 191103.
- (14) Galego, J.; Climent, C.; Garcia-Vidal, F. J.; Feist, J. *Phys. Rev. X* **2019**, *9*, 021057.
- (15) del Pino, J.; Feist, J.; Garcia-Vidal, F. J. *New J. Phys.* **2015**, *17*, 053040.
- (16) Campos-Gonzalez-Angulo, J. A.; Ribeiro, R. F.; Yuen-Zhou, J. *Nat Commun* **2019**, *10*, 4685.
- (17) Li, T. E.; Nitzan, A.; Subotnik, J. E. *J. Chem. Phys.* **2020**, *152*, 234107.
- (18) Vurgaftman, I.; Simpkins, B. S.; Dunkelberger, A. D.; Owrutsky, J. C. *J. Phys. Chem. Lett.* **2020**, 3557–3562.
- (19) Li, X.; Mandal, A.; Huo, P. *Nat Commun* **2021**, *12*, 1315.
- (20) Yang, P.-Y.; Cao, J. *J. Phys. Chem. Lett.* **2021**, *12*, 9531–9538.
- (21) Mandal, A.; Li, X.; Huo, P. *J. Chem. Phys.* **2022**, *156*, 014101.

- (22) Hynes, J. *J. Stat. Phys.* **1986**, *42*, 149–168.
- (23) Flick, J.; Ruggenthaler, M.; Appel, H.; Rubio, A. *PNAS* **2017**, *114*, 3026–3034.
- (24) Haugland, T. S.; Schäfer, C.; Ronca, E.; Rubio, A.; Koch, H. *J. Chem. Phys.* **2021**, *154*, 094113.
- (25) Sidler, D.; Ruggenthaler, M.; Appel, H.; Rubio, A. *J. Phys. Chem. Lett.* **2020**, *11*, 7525–7530.
- (26) Power, E. A.; Zienau, S.; Massey, H. S. W. *Philos. Trans. R. Soc. Lond. Ser. Math. Phys. Sci.* **1959**, *251*, 427–454.
- (27) Schäfer, C.; Ruggenthaler, M.; Rokaž, V.; Rubio, A. *ACS Photonics* **2020**, *7*, 975–990.
- (28) Climent, C.; Feist, J. *Phys. Chem. Chem. Phys.* **2020**, *22*, 23545–23552.
- (29) Richter, F.; Hochlaf, M.; Rosmus, P.; Gatti, F.; Meyer, H.-D. *J. Chem. Phys.* **2004**, *120*, 1306–1317.
- (30) Richter, F.; Rosmus, P.; Gatti, F.; Meyer, H.-D. *J. Chem. Phys.* **2004**, *120*, 6072–6084.
- (31) Richter, F.; Gatti, F.; Léonard, C.; Le Quéré, F.; Meyer, H.-D. *J. Chem. Phys.* **2007**, *127*, 164315.
- (32) Montgomery, J. A.; Chandler, D.; Berne, B. J. *J. Chem. Phys.* **1979**, *70*, 4056–4066.
- (33) Rosenberg, R. O.; Berne, B. J.; Chandler, D. *Chemical Physics Letters* **1980**, *75*, 162–168.
- (34) Kuharski, R. A.; Chandler, D.; Montgomery, J. A.; Rabii, F.; Singer, S. J. *J. Phys. Chem.* **1988**, *92*, 3261–3267.
- (35) Li, T. E.; Subotnik, J. E.; Nitzan, A. *Proc. Natl. Acad. Sci.* **2020**, *117*, 18324–18331.

- (36) Wang, D. S.; Neuman, T.; Yelin, S. F.; Flick, J. *ArXiv210906631 Nlin Physicsphysics Physicsquant-Ph* **2021**.
- (37) Chandler, D. *Introduction to Modern Statistical Mechanics*; Oxford University Press: New York, 1987.
- (38) Berne, B. J.; Borkovec, M.; Straub, J. E. *J. Phys. Chem.* **1988**, *92*, 3711–3725.
- (39) Eyring, H. *J. Chem. Phys.* **1935**, *3*, 107–115.
- (40) Hänggi, P.; Talkner, P.; Borkovec, M. *Rev. Mod. Phys.* **1990**, *62*, 251–341.
- (41) Masgrau, L.; González-Lafont, À.; Lluch, J. M. *J. Phys. Chem. A* **2002**, *106*, 11760–11770.
- (42) Miller, W. H. *J. Am. Chem. Soc.* **1979**, *101*, 6810–6814.
- (43) Matzkies, F.; Manthe, U. *J. Chem. Phys.* **1998**, *108*, 4828–4836.
- (44) Vendrell, O. *Phys. Rev. Lett.* **2018**, *121*, 253001.
- (45) Schäfer, C.; Flick, J.; Ronca, E.; Narang, P.; Rubio, A. *ArXiv210412429 Phys. Physicsquant-Ph* **2021**.
- (46) Li, T. E.; Nitzan, A.; Subotnik, J. E. *Angew. Chem. Int. Ed.* **2021**, *60*, 15533–15540.

**Supporting Information:**  
**On the Suppression and Enhancement of**  
**Thermal Chemical Rates in a Cavity**

Jing Sun\* and Oriol Vendrell\*

*Theoretische Chemie, Physikalisch-Chemisches Institut, Universität Heidelberg,  
69120 Heidelberg, Germany*

E-mail: [jing.sun@pci.uni-heidelberg.de](mailto:jing.sun@pci.uni-heidelberg.de); [oriol.vendrell@uni-heidelberg.de](mailto:oriol.vendrell@uni-heidelberg.de)



# Calculation of the transmission coefficient

Starting from the general definition of the forward reaction rate

$$K(t) = x_{cis}^{-1} \langle \dot{\tau}(0) \delta[\tau(0) - \tau^\ddagger] \theta[\tau(t)] \rangle \quad (1)$$

and its TST limit

$$K_{TST} = x_{cis}^{-1} \langle \dot{\tau}(0^+) \delta[\tau(0) - \tau^\ddagger] \rangle, \quad (2)$$

which integrates only over the forward flux assuming it all leads to products, the transmission coefficient

$$\kappa(t) = \frac{\langle \dot{\tau}(0) \delta[\tau(0) - \tau^\ddagger] \theta[\tau(t)] \rangle}{\langle \dot{\tau}(0^+) \delta[\tau(0) - \tau^\ddagger] \rangle} \quad (3)$$

can be defined.  $\kappa$  contains all dynamical information that escapes the zero-recrossing,  $\kappa = 1$  TST limit. The rate  $K = \kappa K_{TST}$ , where  $\kappa \equiv \lim_{t \rightarrow \infty} \kappa(t)$ , is the exact classical forward rate (if it exists: for very low barriers between two meta-stable configurations  $\kappa$  tends quickly to 0 and no rate can be defined).

$\kappa(t)$  is calculated as follows: For every set of parameters ( $g, \omega_{cav}, N$ ) considered, a Metropolis sampling in conformation space samples the canonical distribution with probability proportional to  $\exp -\beta V(\vec{R}^\ddagger)$ , with  $\beta^{-1} = k_B T$  and  $T = 300$  K. In  $\vec{R}^\ddagger$ , the torsion coordinate is constrained to its transition state (TS) value  $\tau^\ddagger$ , and the corresponding configurational space is therefore 5-dimensional. In the Metropolis sampling, the step size of the random moves is adjusted in an initial burn-in phase to attain an acceptance ratio of 40%. To reduce the correlation of contiguous samples in the generated Markov chain, only one in every 5 samples is kept. Finally,  $5 \times 10^5$  initial configurations are collected and split in 5 independent batches. The corresponding velocities are initialized from a Maxwell-Boltzmann distribution. The classical equations of motion of the system plus cavity are integrated in

the Newtonian formulation using the velocity-Verlet algorithm with a time-step of 1 fs. The standard deviation of each run is determined over the averages of the 5 independent batches.

## Transition state theory rates

Although TST rates can be directly evaluated using Eq. 2, we find it more convenient to use Eyring’s equation

$$k_{TST} = \frac{1}{\beta h} \frac{Z^\ddagger}{Z^R} e^{-\beta \Delta E} \quad (4)$$

where  $Z^\ddagger$  and  $Z^R$  correspond to the partition function of transition state (TS) and reactant, respectively. The partition functions are evaluated as usual by optimizing the *cis* and TS stationary point geometries for each set of parameters and constructing and diagonalizing the Hessian matrix to obtain separable normal modes. Finally, the quantum mechanical partition functions for the oscillators in the reactants and TS are evaluated using the well-known textbook expressions.  $\Delta E$  in Eq. 4 corresponds to the difference of zero-point energies between reactants and TS.

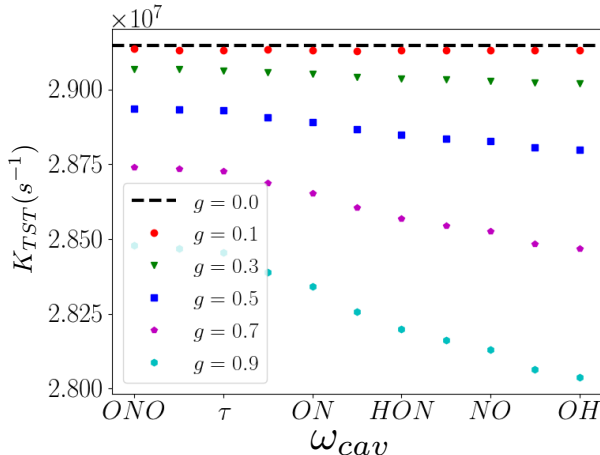


Figure S1: Transition state theory rates calculated with Eyring’s equation. The frequencies for  $\omega_{cav}$  are taken to be resonant with the harmonic vibrational frequencies of HONO. Their values are given in the caption to Fig. 4 in the main text.

# HONO permanent dipole

The permanent dipole moment of HONO has been evaluated at the MP2 level of theory using the atomic basis 6-311g++(d,p).

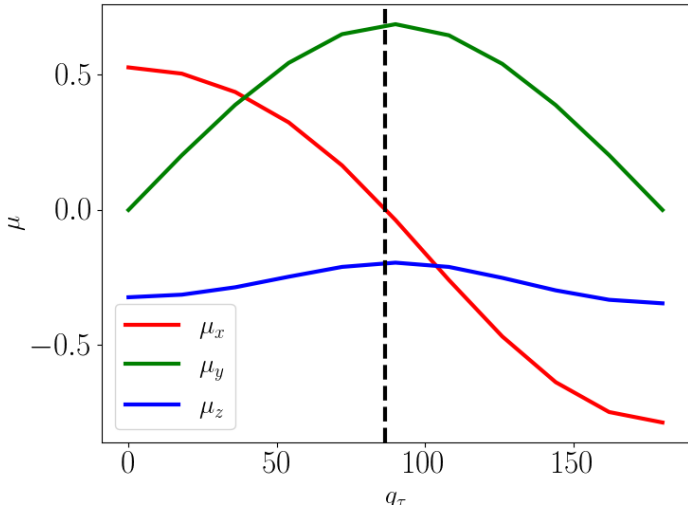


Figure S2: Permanent dipole of the HONO molecule in atomic units as a function of the torsion coordinate  $\tau$ . The axes are referred to the molecular frame axis in Fig. 1 of the main text.

## Calculations with a bath

For the calculations with a bath coupled to the reaction coordinate, the bath Hamiltonian is modeled as

$$\hat{H}_{bath} = \sum_k \frac{p_k^2}{2m_k} + \frac{m_k \omega_k^2}{2} \left[ q_k + \frac{c_k}{m_k \omega_k^2} (R_{rxn} - R_{rxn}^\ddagger) \right]^2, \quad (5)$$

which describes the interaction between the reaction coordinate ( $R_{rxn}$ ) of the system and bath modes, which linearly grows with displacements from the TS.  $q_k$  denotes the coordinate of the  $k$ -th bath mode with a conjugate momentum  $p_k$  and mass  $m_k = 1836$  a.u.. The coupling constants  $c_k$  and the frequencies  $\omega_k$  are chosen to represent an Ohmic spectral

density

$$J(\omega) = \frac{\pi}{2} \sum_k \frac{c_k^2}{m_k \omega_k} \delta(\omega - \omega_k) = \frac{\pi}{2} \hbar \xi \omega e^{-\omega/\omega_p}, \quad (6)$$

where  $\omega_p$  is set to be 170.6 meV and  $\xi$  is a unit-less factor ( $\xi = 1.74$  in our calculation).

Hence, one can derive  $\omega_k$  and  $c_k$  from

$$\omega_k = -\omega_p \ln\left(1 - k \left(\frac{\omega_N}{\omega_p}\right)\right), \quad (7)$$

and

$$c_k = \sqrt{\xi \hbar \omega_N m_k \omega_k}, \quad (8)$$

where  $\omega_N = \frac{\omega_p}{N}(1 - e^{-\omega_m/\omega_p})$ . For production calculations we used  $N = 20$  bath modes, but we tried with up to  $N = 80$  modes to check for convergence and the system's observables remained unchanged.  $\omega_N$  denotes the largest frequency in the bath ( $\omega_N = 5\omega_p$ ).